Int J Adv Manuf Technol (2017) 91:2869–2874
DOI 10.1007/s00170-017-0007-9

ORIGINAL ARTICLE

Optimization of rotation speed ratio in dual-rotation friction stir welding by finite element method

X. M. Liu[1] · X. M. Zhang[1] · J. S. Yao[2] · Y. H. Yin[2] · P. Y. Xia[2]

Received: 6 August 2016 / Accepted: 4 January 2017 / Published online: 12 January 2017

Abstract Dual-rotation friction stir welding (DR-FSW) is a new variant technique of friction stir welding. By adopting different rotation speeds for the pin and shoulder, the temperature gradient can be adjusted to help decrease overheat and the dissolution of the strengthening precipitates and produces good joints for some cases, such as thick plates. In this study, by thermal-mechanical coupling method, with the help of finite element software—DEFORM-3D, the temperature field of workpieces in DR-FSW for an 80-mm-thick 5A06 aluminum alloy was simulated, and the temperature gradients at different rotation speed ratios were calculated and analyzed. Better process parameters could be concluded using optimization. In our simulation, the rotation ratio of 200 rpm for the shoulder and 400 rpm for the pin in the first group achieved the gentlest temperature gradient in thickness direction with a temperature difference between the upper and lower surfaces of less than 30 °C. The study represents a practical reference for choosing process parameters in the actual DR-FSW process.

Keywords Dual-rotation friction stir welding · Finite element method · DEFORM-3D · Temperature gradient

✉ X. M. Liu
xuemei_buaa@sdu.edu.cn

[1] Key Laboratory for Liquid-Solid Structural Evolution & Processing of Materials Ministry of Education, Shandong University, Jinan 250061, China

[2] Shanghai Aerospace Equipments Manufacturer, Shanghai 200045, China

1 Introduction

Since friction stir welding (FSW) was invented by The Welding Institute (TWI) in 1991 [1–3], it was deemed effective for joining hard-to-weld metals [4]. Many advantages of FSW such as energy-efficiency, environmental friendliness, and versatile green [2] have attracted more researchers, and it has been widely used in more conditions [5–9]. At the same time, some new variant techniques were developed such as bobbin tool friction stir welding [10, 11], friction stir spot welding [12, 13], and friction plug welding [14–16]. Among these methods, the dual-rotation friction stir welding is a relatively new variant technique where the tool is divided into two separate parts, that is, the pin and the shoulder can rotate at different speeds [17]. Yet in conventional FSW, the tool is built as a whole, and the pin and the shoulder rotate at the same speed such that the heat produced by the shoulder of the larger diameter accounts for a large proportion of the whole frictional heat [18, 19]. In this case, there is a larger temperature gradient in the thickness direction of the workpiece, especially for thicker plates. To weld thicker plates successfully, a higher temperature near the shoulder is required and often leads to the direct overheating and dissolution of the strengthening precipitates and results in poor joint properties [20–22]. With dual-rotation friction stir welding, the overheating or incipient melting that greatly deteriorates the microstructures and mechanical properties can be reduced largely because the temperature near the shoulder can be lowered by decreasing the rotating speed of the shoulder [23]. Li et al. [24, 25] successfully performed the reverse dual-rotation friction stir welding (RDR-FSW) of AA2219-T6 and compared the microstructures and mechanical properties of its different welding parameters.

They also analyzed the effects of reverse-rotating the shoulder on structures and joint properties. Simulations were also conducted to model the material flow and heat transfer in RDR-FSW [26–28].

Previous research has shown that obtaining satisfied joints requires a median temperature (i.e., neither too high nor too low) near the shoulder such that there is a better rotational speed ratio in dual-rotation friction stir welding for specific cases. The present study used the finite element method to simulate and analyze the temperature gradients at different rotational speed ratios and, by optimization, provided better process parameters that can represent a practical reference for choosing the process parameters in the actual dual-rotation friction stir welding process.

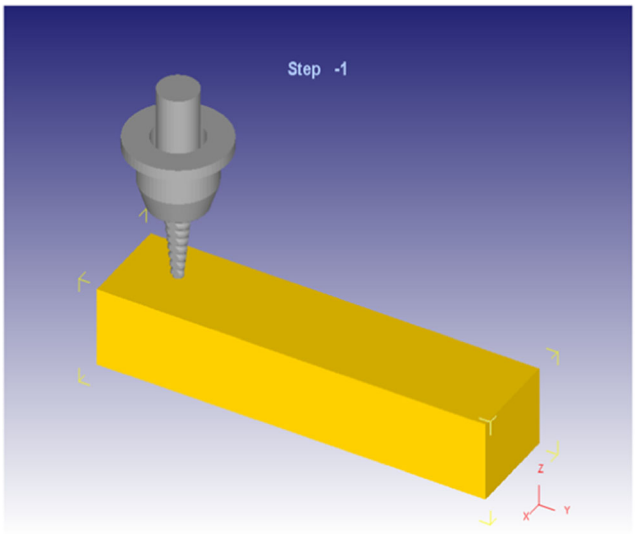

Fig. 2 Assembly model of the workpiece and tool

2 Numerical modeling

2.1 Geometric model

The geometric model of the workpiece was set up in DEFORM-3D. For simplification and to avoid misconvergence, the workpiece was simplified to be one whole plate with a geometric size of 500 mm × 120 mm × 80 mm.

The geometric model of the tool was set up using UG software and was then exported to DEFORM-3D, as illustrated in Fig. 1. The outer diameters of the sub-size concave shoulder and the assisted shoulder are 44.83 and 50 mm, respectively, while the root diameter of the pin is 33.92 mm.

Figure 2 is the assembly model showing the starting point of welding set to a 60-mm distance from the workpiece's length boundary, a 0.8° tool tilt angle, and a pin depth of 77.46 mm.

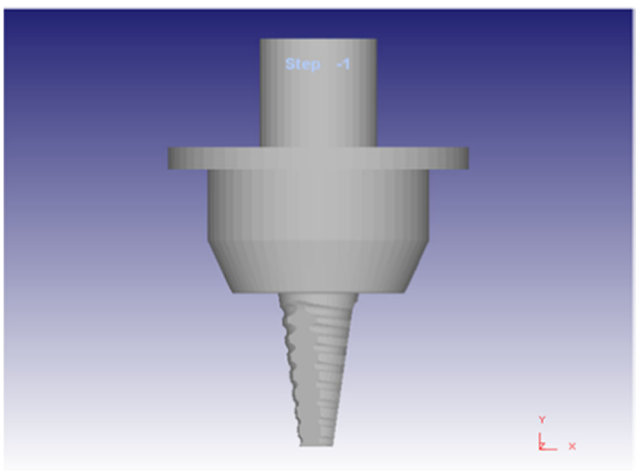

Fig. 1 Geometric model of the tool

2.2 Mesh generation

A non-uniform mesh was adopted to improve calculation accuracy and time efficiency. Altogether, 25,000 meshes were adopted. Different mesh generations were used for the first period, wherein the tool was screwed down, and for the second period, where the tool had a transverse movement. Figure 3 shows the mesh scheme for the first period with only a cylinder around the tool which adopted fine mesh. In the second period, both the cylinder and the

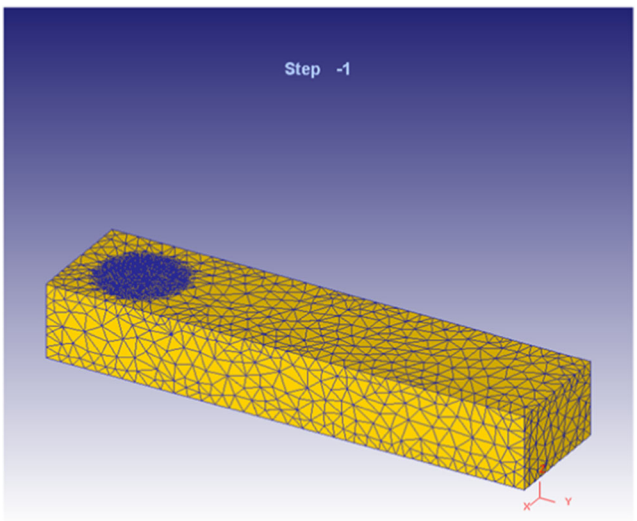

Fig. 3 Mesh scheme for the first period of tool's screw down

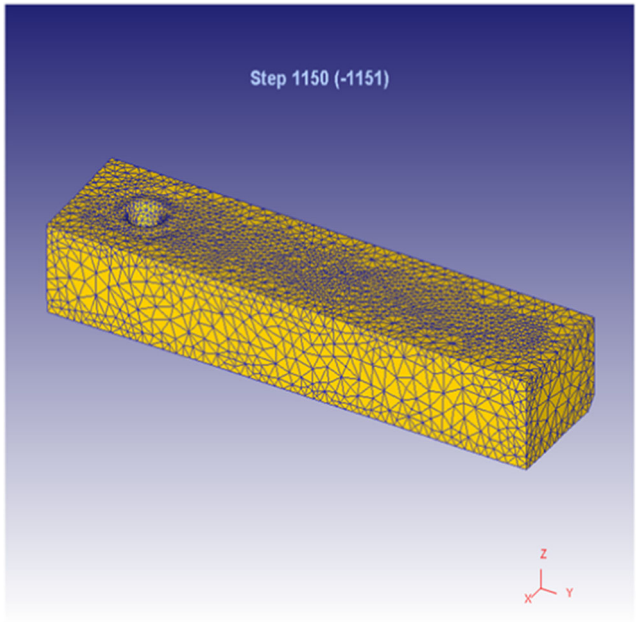

Fig. 4 Mesh scheme for the second period of tool's transverse movement

cuboid are present such that the tool would move inside the adopted fine mesh (Fig. 4). A mesh deforming ratio exceeding 0.7, which is the remeshing criteria, triggers remeshing.

2.3 Material properties and governing equations

A rigid tool was assumed given that the tool wear loss was neglected during the process. A rigid-viscoplastic aluminum alloy (5A06) was assumed for the welding process such that, in the simulation, the process was simplified to be a non-isothermal forming problem with heat transfer analysis with a rigid tool and a rigid-viscoplastic workpiece.

The thermophysical parameters of the workpiece (5A06 aluminum alloy) were obtained from the material library of the DEFORM-3D software, with a focus on the plastic flow data. These data govern the deformation and flow behavior of the workpiece undergoing permanent deformation. In the simulation, the flow stress is a function of the strain, strain rate, and temperature. That is,

$$\overline{\sigma} = f\left(\overline{\varepsilon}, \dot{\overline{\varepsilon}}, T\right) \tag{1}$$

where $\overline{\sigma}$ is the flow stress, $\overline{\varepsilon}$ is the effective plastic strain, $\dot{\overline{\varepsilon}}$ is the effective strain rate, and T is the temperature.

The process of friction stir welding was considered a coupled thermomechanical problem that could be treated as a matter of unsteady heat exchange with an inner heat source. The fundamental equation of the heat condition with changeable thermal properties can be expressed as the following three-dimensional (3D), unsteady equation, which was illustrated by an earlier study [29]:

$$\rho c \frac{\partial T}{\partial t} = k\left(\frac{\partial^2 T}{\partial r^2} + \frac{1}{r}\frac{\partial T}{\partial r} + \frac{\partial^2 T}{\partial z^2}\right) + \dot{q} \tag{2}$$

where ρ, c, and k are the density, specific heat, and thermal conductivity of the workpiece material, respectively, and $\dot{q}$ is the internal energy rate.

The common properties of the 5A06 aluminum alloy at room temperature are listed in Table 1.

Table 1 Density, specific heat capacity, and thermal conductivity of 5A06 aluminum alloy at 20 °C

Properties	ρ/(g cm^{-3})	c/(J kg^{-1} K^{-1})	k/(W m^{-1} K^{-1})
5A06	2.63	904	120

2.4 Boundary conditions

To avoid tool influence on the workpiece's movement, the node velocity in the workpiece's side faces were specified. During the first period of tool's screw down, there was no movement in the x-, y-, and z-directions of the nodes and sides. During the second period of tool's transverse movement, there was no movement in the x- and z-directions, although a velocity of 0.3 mm/s was set in the y-direction.

The friction interface between the tool and the workpiece was treated as the heat-generating face. The other faces that contacted the surroundings were treated as the heat-dissipating faces. In the simulation, water-cooling in

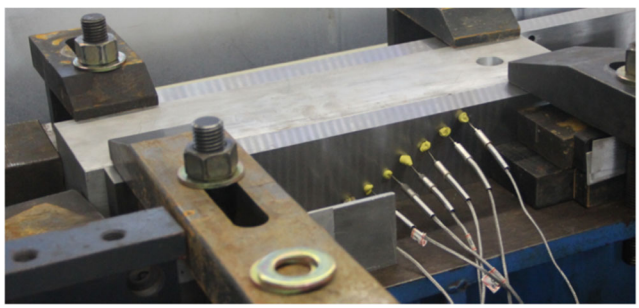

Fig. 5 The experimental equipment setup

the real process was regarded as a cooling resource acting on the faces of the contacted surroundings. The amount of cooling resource was calculated using the corresponding heat transfer formula.

3 Experimental work

Experimental work was performed to test the simulation results, wherein thermocouples were used to measure the temperatures, and a two-plated device was clamped the workpiece firmly to control and reduce the welding deformation in FSW, as illustrated in Fig. 5. The size of the workpiece with additional plates was the same as the workpiece used in simulations for two reasons. Firstly, this reduces the amount of calculations required in the simulation and would result in more accurate test simulation results. Secondly, this ensures more convenient and efficient thermocouple installations. Seven thermocouples were installed altogether at 10-mm intervals in the direction of the thickness (z-axis) and at a 40-mm instance from the outer sides of the additional plates (Fig. 5). In the experiments, a hole was preset to avoid too much material being forced out, thereby affecting the judgments of the screw down.

In the experiment, the pin rotated at 400 rpm and the shoulder rotated at 200 rpm. The plunge depth of shoulder was 1–1.5 mm and the tool's transverse speed was 18 mm/min during the second period. During the welding process, cooling water was poured to the weld continuously to avoid overheating.

4 Results and discussion

4.1 Temperature changes with time

During testing, the lowest couple dropped off and six temperature points were recorded. Figure 6 is the comparison chart of the temperature curves changing with time for six spots between the experimental and simulation results. Among these curves, curves 1–6 are the experimental results and curves 1′–6′ are the simulation results, correspondingly. Figure 6 depicts similar developing trends between the similar and experimental results for each of the six points, such that the highest temperatures are approximately the same. The large thickness (80 mm) of the workpiece could not avoid fluctuations and required a finer mesh size even with the large amounts of meshes and non-uniform mesh adopted. This was especially true for the spots in the experiment, which is a bit farther from the weld middle and is not in the zone of the finest meshes.

4.2 Influence of rotation rate ratio on temperature field

Three different groups of rotation rate ratios were set, namely 200 rpm for the shoulder and 400 rpm for the pin in the first group, 200 rpm for the shoulder and 500 rpm for the pin in the second group, and 100 rpm for the shoulder and 500 rpm for the pin in the third group. The other conditions were the same, such that the welding speeds were all set at 0.3 mm/s.

At 39 s, the tool was screwed to the bottom and the temperature field achieved a quasi-steady state, although

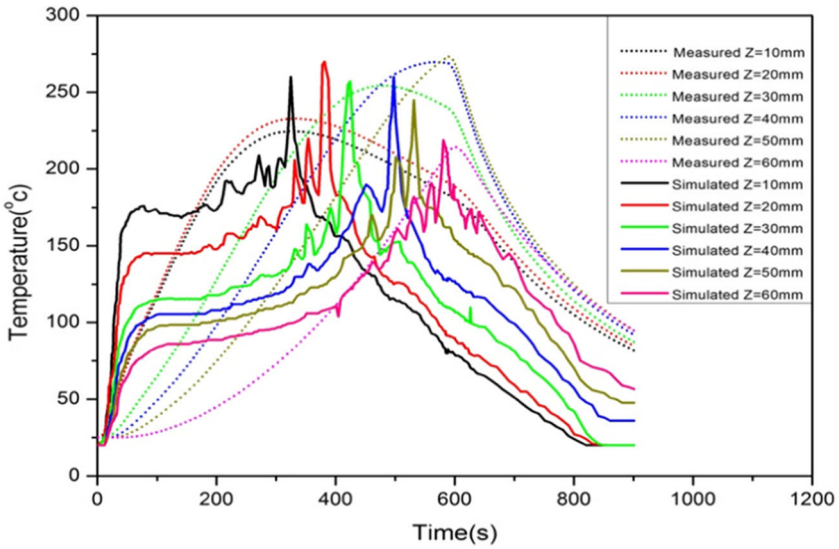

Fig. 6 Comparison chart of temperature changes with time for six spots between the experimental and simulation results

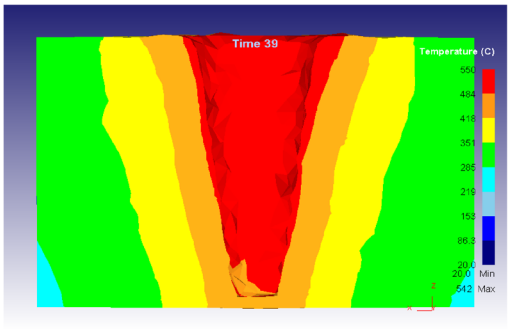

(a) The first group (200 rpm for the shoulder and 400 rpm for the pin)

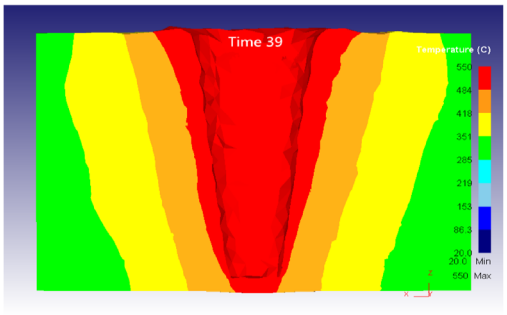

(b) The second group (200 rpm for the shoulder and 500 rpm for the pin)

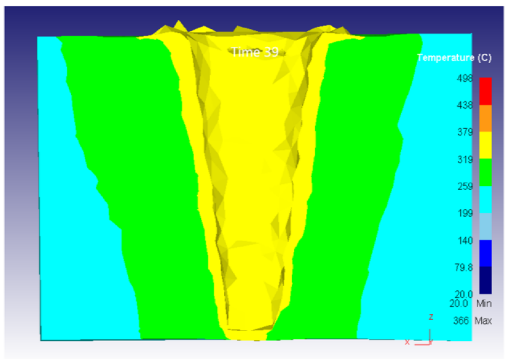

(c) The third group (100 rpm for the shoulder and 500 rpm for the pin)

Fig. 7 Cross-section temperature clouds of the workpiece at 39 s for different rotation rate ratio conditions

the second period of tool transverse movement had not started. Therefore, the cross-sectional temperature cloud of the workpiece was captured at 39 s for different rotation rate ratio conditions, as illustrated in Fig. 7.

Figure 7 shows a lack of significant difference in the temperature distribution between the first and second groups, whereas the third rotation rate ratio condition illustrates a much lower temperature than abovementioned conditions. Therefore, it can be concluded that the heat generated by the shoulder still shares a large proportion in the FSW of the thicker plate.

At certain times, the temperature around the tool was captured for points to get temperature gradients in the

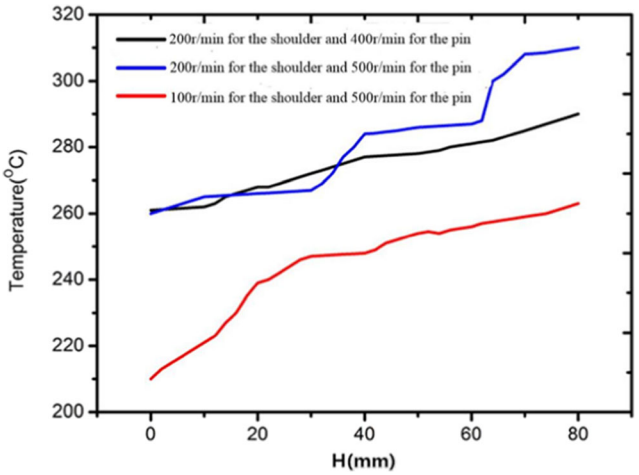

Fig. 8 Gradient of temperature distribution in the thickness direction for different rotation rate ratio conditions (t = 167 s)

thickness direction at different rotation speed ratios. At a time of 167 s in the second period of the steady tool transverse movement, 5-mm distances were collected from the temperature points to the weld center as well as in the 2-mm intervals in thickness direction between temperature points.

Figure 8 illustrates the temperature distribution gradient in the thickness direction for different rotation rate ratio conditions. The results show the temperature distribution gradient in the thickness direction for the first group (200 rpm for the shoulder and 400 rpm for the pin) as the gentlest and the temperature difference between the upper and lower surface remaining below 30 °C. Therefore, successful welding can be achieved, such that the lower surface maintains its plasticity, when the upper surface is maintained at a relatively low temperature to avoid overheating and poor welding quality.

5 Conclusions

(1) The simulation results of the temperature changes with time for the six points showed a similar trend with that of the experimental results, thereby validating the effectiveness of the simulation model in providing guidance for the real process.

(2) The cross-section temperature clouds of the workpiece at 39 s for the different rotation rate ratio conditions showed that the heat generated by the shoulder still provided a large proportion of whole heat for welding during dual-rotation friction stir welding.

(3) In our simulation, the rotation ratio of 200 rpm for the shoulder and 400 rpm for the pin in the first group had the gentlest temperature gradient in the thickness

direction, whereas the temperature difference between the upper and lower surfaces was below 30 °C.

Acknowledgements We thank LetPub (www.letpub.com) for its linguistic assistance during the preparation of this manuscript.

References

1. Nandan R, Debroy T, Bhadeshia HKDH (2008) Recent advances in friction-stir welding-process, weldment structure and properties. Prog Mater Sci 53:980–1023
2. He XC, Gu FS, Ball A (2014) A review of numerical analysis of friction stir welding. Prog Mater Sci 65:1–66
3. Thomas WM, Nicholas ED, Needham JC, Murch MG, Temple-Smith P, Dawes CJ (1991) Friction stir butt welding. International Patent Application No. PCT/GB92/02203
4. Mishra RS, Ma ZY (2005) Friction stir welding and processing. Mater Sci Eng R 50:1–78
5. Starke EA, Staley JT (1996) Application of modern aluminum alloys to aircraft. Prog Aerosp Sci 32:131–172
6. Heinz A, Haszler A, Keidel C, Moldenhauer S, Benedictus R, Miller WS (2000) Recent development in aluminium alloys for aerospace applications. Mater Sci Eng A 280:102–107
7. Longhurst WR, Cox CD, Gibson BT, Cook GE, Strauss AM, Wilbur IC, Osborne BE (2016) Development of friction stir welding technologies for in-space manufacturing. Int J Adv Manuf Technol. doi:10.1007/s00170-016-9362-1
8. Eslami S, Tavares PJ, Moreira PMGP (2016) Friction stir welding tooling for polymers: review and prospects. Int J Adv Manuf Technol. doi:10.1007/s00170-016-9205-0
9. Papahn H, Bahemmat P, Haghpanahi M, Sommitsch C (2015) Study on governing parameters of thermal history during underwater friction stir welding. Int J Adv Manuf Technol 78:1101–1111
10. Tomohiko G, Hiroaki S, Daisuke T, Hideaki S, Takeshi Y, Hidenori H (2005) Highly reliable tank structure of H-IIB launch vehicle. Mitsubishi Heavy Industries Ltd. Technical Review 42:1–4 http://www.mhi.co.jp/technology/review/pdf/e425/e425234.pdf
11. Guan Q, Luan GH (2008) The current status and development of FSW. http://info.mt.hc360.com/2008/10/09093845905.shtml
12. Sakano R, Murakami K, Yamashita K, Hyoe T, Fujimoto M, Inuzuka M, Nagao Y, Kashiki H (2001) Development of spot FSW robot system for automobile body members. In: Proceedings of the 3rd International Symposium of Friction Stir Welding, Kobe
13. Chen YC, Gholinia A, Prangnell PB (2012) Interface structure and bonding in abrasion circle friction stir spot welding: a novel approach for rapid welding aluminium alloy to steel automotive sheet. Mater Chem Phys 134:459–463
14. Luan GH, Ji YJ, Dong CL, Ma XS (2006) Microstructure of LY12 aluminium alloy welded joint of friction plug welding. Trans China Weld Inst 27:1–3
15. ZhaoYH LJD, Zhang LN, Sun ZS, Wang GQ (2010) Study on friction plug welding of 2014 aluminum alloy FSW joint. J Aeronaut Mater 30:41–46
16. Chen H , Liu JD, Zhang LN, Zhang YK, Du YF (2007) Study on friction plug welding of aluminum alloy. In: International Astronautical Federation - 58th International Astronautical Congress, Hyderabad
17. Thomas WM, Norris IM, Staines DG, Watts, ER (2005) Friction stir welding—process developments and variant techniques. In: The SME Summit 2005, Oconomowoc, Milwaukee
18. Schmidt H, Hattel J, Wert J (2004) An analytical model for the heat generation in friction stir welding. Model Simul Mater Sci Eng 12: 143–157
19. Neto DM, Neto P (2013) Numerical modeling of friction stir welding process: a literature review. Int J Adv Manuf Technol 65: 115–126
20. Park SHC, Sato YS, Kokawa H (2003) Effect of micro-texture on fracture location in friction stir weld of Mg alloy AZ61 during tensile test. Scripta Mater 49:161–166
21. Sato YS, Kokawa H, Enomoto M, Jogan S (1999) Microstructural evolution of 6063 aluminum during friction-stir welding. Metall Mater Trans A 30:2429–2437
22. Oertelt G, Babu SS, David SA, Kenik EA (2001) Effect of thermal cycling on friction stir welds of 2195 aluminum alloy. Weld J 80: 71–79
23. Shi L, Wu CS, Liu HJ (2015) The effect of the welding parameters and tool size on the thermal process and tool torque in reverse dual-rotation friction stir welding. Int J Mach Tools Manuf 91:1–11
24. Li JQ, Liu HJ (2013) Effects of welding speed on microstructures and mechanical properties of AA2219-T6 welded by the reverse dual-rotation friction stir welding. Int J Adv Manuf Technol 68: 2071–2083
25. Li JQ, Liu HJ (2014) Optimization of welding parameters for the reverse dual-rotation friction stir welding of a high-strength aluminum alloy 2219-T6. Int J Adv Manuf Technol 76:1469–1478
26. Shi L, Wu CS, Liu HJ (2014a) Modeling the material flow and heat transfer in reverse dual-rotation friction stir welding. J Mater Eng Perform 23:2918–2929
27. Shi L, Wu CS, Liu HJ (2014b) Modeling material plastic flow and thermal field in reverse dual-rotation friction stir welding. Chin J Mech Eng 50:140–146
28. Shi L, Wu CS, Liu HJ (2014c) Numerical analysis of heat generation and temperature field in reverse dual-rotation friction stir welding. Int J Adv Manuf Technol 74:319–334
29. Liu XM, Yao JS, Cai Y, Meng H, Zou ZD (2013) Simulation on the temperature field of bobbin tool friction stir welding of AA 2014 aluminium alloy. Appl Mech Mater 433-435:2091–2095